

Deep Ensemble Shape Calibration: Multi-Field Post-hoc Calibration in Online Advertising

Shuai Yang
Shopee Discovery Ads
Beijing, China

Hao Yang
Shopee Discovery Ads
Beijing, China

Zhuang Zou
Shopee Discovery Ads
Beijing, China

Linhe Xu
Shopee Discovery Ads
Beijing, China

Shuo Yuan
Shopee Discovery Ads
Beijing, China

Yifan Zeng
Shopee Discovery Ads
Beijing, China

ABSTRACT

In the e-commerce advertising scenario, estimating the true probabilities (known as a calibrated estimate) on Click-Through Rate (CTR) and Conversion Rate (CVR) is critical and can directly affect the benefits of the buyer, seller and platform.

Previous research has introduced numerous solutions for addressing the calibration problem. These methods typically involve the training of calibrators using a validation set and subsequently applying these calibrators to correct the original estimated values during online inference. However, what sets e-commerce advertising scenarios is the challenge of multi-field calibration. Multi-field calibration can be subdivided into two distinct sub-problems: **value** calibration and **shape** calibration. **Value** calibration is defined as no over- or under-estimation for each value under concerned fields (such as the average of pCTR should equal to the CTR for value "women's shoes" in the field "category", in the advertising context, the number of fields can range from dozens to even hundreds). **Shape** calibration is defined as no over- or under-estimation for each subset of the pCTR within the specified range under condition of concerned fields. In order to achieve **shape** calibration and **value** calibration, it is necessary to have a strong data utilization ability. Because the quantity of pCTR specified range for single field-value (such as user ID and item ID) sample is relative small, which makes the calibrator more difficult to train. However the existing methods cannot simultaneously fulfill both value calibration and shape calibration.

To solve these problems, we propose a new method named Deep Ensemble Shape Calibration (DESC)¹. We introduce innovative basis calibration functions, which enhance both function expression capabilities and data utilization by combining these basis calibration functions. A significant advancement lies in the development of an allocator capable of allocating the most suitable shape calibrators to different estimation error distributions within diverse fields and values. Finally, we achieve significant improvements in both public

data and industrial data, and on online experiments we get +2.5% of CVR and +4.0% of GMV (Gross Merchandise Volume).

KEYWORDS

Multi-Field Calibration, Basis Calibration Function, Field-aware Attention

ACM Reference Format:

Shuai Yang, Hao Yang, Zhuang Zou, Linhe Xu, Shuo Yuan, and Yifan Zeng. 2018. Deep Ensemble Shape Calibration: Multi-Field Post-hoc Calibration in Online Advertising. In *Proceedings of Make sure to enter the correct conference title from your rights confirmation email (Conference acronym 'XX)*. ACM, New York, NY, USA, 9 pages. <https://doi.org/XXXXXXX.XXXXXXX>

1 INTRODUCTION

Estimating CTR and CVR is a crucial technology in e-commerce advertising domains [2–6, 9, 13, 21, 25–27, 29, 32, 34]. Accurate prediction of CTR (pCTR) and CVR (pCVR) is essential, as it necessitates precision not only in ranking but also in absolute values.

However, recent studies [1, 8, 15, 22] have revealed that numerous established machine learning techniques, particularly deep learning methods extensively applied in the fields of e-commerce advertising, often yield inadequately calibrated probability predictions.

In previous research, there are many solutions to solve the calibration problem. These methods learn calibrator through the validation set, and then use the calibrator to correct the original estimated values in the online inference stage. These methods can be categorized into parameter methods (including Platt Scaling [24], Temperature scaling [8], Beta calibration [17], Gamma calibration [19] and Dirichlet calibration [16]), non-parameter methods (such as Histogram Binning [30] and Isotonic Regression [31]) and hybrid methods. Hybrid methods encompass both non-field-aware [14, 18, 33] and field-aware approaches [12, 23, 28].

However, what sets apart e-commerce advertising scenarios is the challenge of multi-field calibration, which means that for each pCTR range in each value under each concerned field the pCTR should be calibrated. Multi-field calibration can be subdivided into two distinct sub-problems: **value** calibration and **shape** calibration. **Value** calibration is defined as no over- or under-estimation each value under concerned fields (such as average of pCTR should equal to the CTR for value "women's shoes" in the field "category", in the e-commerce advertising context, the number of fields can range from dozens to even hundreds). Figure 1 illustrates the significant inconsistency of over- and under-estimation across different field

¹The code is at <https://github.com/HaoYang0123/DESC>

Permission to make digital or hard copies of all or part of this work for personal or classroom use is granted without fee provided that copies are not made or distributed for profit or commercial advantage and that copies bear this notice and the full citation on the first page. Copyrights for components of this work owned by others than ACM must be honored. Abstracting with credit is permitted. To copy otherwise, or republish, to post on servers or to redistribute to lists, requires prior specific permission and/or a fee. Request permissions from permissions@acm.org.

Conference acronym 'XX, June 03–05, 2018, Woodstock, NY

© 2018 Association for Computing Machinery.
ACM ISBN 978-1-4503-XXXX-X/18/06...\$15.00
<https://doi.org/XXXXXXX.XXXXXXX>

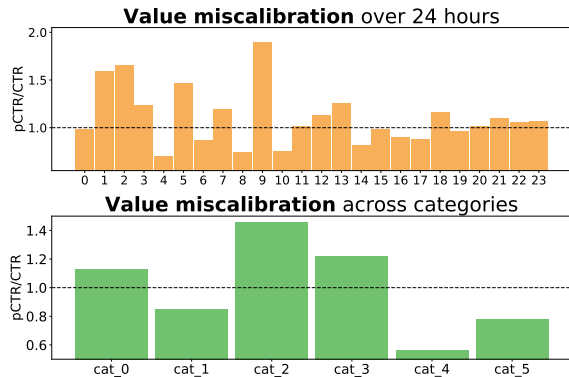


Figure 1: Examples to show significant variations in value miscalibration among different fields and values.

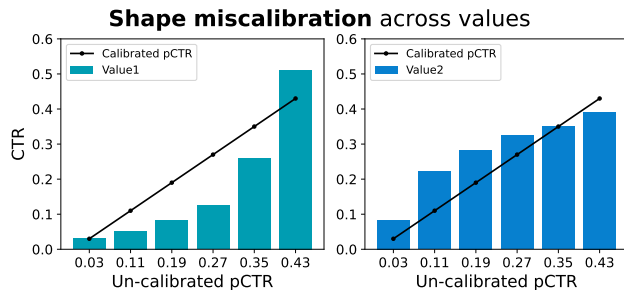


Figure 2: Examples to show significant variations in shape miscalibration among different values within the same field.

values. **Shape** calibration is defined as no over- or under-estimation for each subset of the pCTR within the specified range for each value under concerned fields. Take Figure 2 as an example, Field f has two values: Value1 and Value2, and these two shapes are significantly different. In order to achieve **shape** calibration and **value** calibration, it is necessary to have a strong data utilization ability. Because the samples of the specified pCTR range for single field-value (such as user ID and item ID) are relative small, which makes the calibrator more difficult to train. However, the existing method cannot simultaneously fulfill both value calibration and shape calibration.

For Parameter methods, non-parameter methods and non-field-aware methods, they involve the training of a single calibration function to address the issue of shape miscalibration. These methods focus on shape calibration but not value calibration.

For field-aware methods, they have different emphases, and cannot simultaneously fulfill both value calibration and shape calibration. NeuralCalib/Field-aware Calibration (FAC) [23] places its focus on modeling estimation value biases across various field values, rather than addressing shape miscalibrations. Multiple Boosting Calibration Tree (MBCT) [12] effectively enhances the binning of field values, giving less emphasis to shape miscalibrations. AdaCalib (Ada) [28] can only model shape calibration and value calibration under the condition of a single field.

An analysis of the aforementioned field-aware methods reveals several key observations. Firstly, within a single field, there exists

multiple values. In some cases, the allocation of samples to each field value may be limited, particularly in scenarios involving user ID, item ID and certain sparse cross-features. Consequently, training a calibrator under such limited samples can be challenging. Additionally, field-aware methods often employ a binning strategy, followed by the generation of calibration parameters based on information from two adjacent bins. This approach can lead to a sample isolation issue wherein the parameters of a bin are exclusively influenced by the samples within that bin and its neighboring bins, with no updates from samples in other bins. As a result, these methods can result in suboptimal data utilization.

To solve these above problems, we propose a new method named **Deep Ensemble Shape Calibration (DESC)**. There are four contributions in our work:

- We redefine the multi-field calibration: perform shape calibration and value calibration at the same time.
- We propose the novel basis calibration functions, which can simultaneously improve function expression ability and data utilization through the combination of basis calibration functions.
- We make a breakthrough in putting forward an allocator that can allocate the most suitable shape calibrators for different estimation error distributions on various fields and values.
- Two public datasets and one industrial dataset are tested to show that our proposed DESC method achieves significantly better performance compared with other methods in both calibration metrics and non-calibration metrics. And we get +2.5% of CVR and +4.0% of GMV on the online experiment.

2 RELATED WORKS

With the growing emphasis on improving the reliability and accuracy of machine learning models, several research approaches have emerged. Numerous calibration methods focus on acquiring a mapping function to convert predicted probabilities into observed posterior probabilities, referred to as post-hoc calibration. These studies can be broadly classified into three categories: non-parameter, parameter, and hybrid methods.

2.1 Non-parametric Methods

Non-parametric methods, in contrast, do not rely on any assumptions regarding the distribution of estimates. Examples of non-parametric methods encompass Histogram Binning (HB)[30] and Isotonic Regression (IR) [31]. HB involves sorting the estimated values and then dividing them into bins of equal frequencies or intervals, utilizing the posterior CTR of each bin as a calibration parameter. Building upon this, IR introduces the additional constraint of order preservation. These approach can introduce instability in the bin boundary values.

2.2 Parametric Methods

Parameter methods often rely on specific probability distribution assumptions for deriving mapping functions. Platt Scaling [24], extensively employed in binary classification calibration, assumes a Gaussian distribution with equal variances for both positive and negative classes [19]. For multi-class tasks, Temperature Scaling [8] extends this approach. Beta calibration [17], Gamma calibration [19] and Dirichlet calibration [16] rely on their respective probability

distributions for calibration. Parameter methods are highly reliant on the strong distribution assumption, which can lead to suboptimal performance if the assumption does not hold in practical scenarios.

2.3 Hybrid Methods

Hybrid methods integrate non-parametric and parametric approaches. Based on whether they are applied at the field-level, we further categorize hybrids into two groups: non-field-aware and field-aware methods.

2.3.1 Non-field-aware Methods. Non-field-aware methods encompass three notable approaches: Scaling-binning [18], Smooth Isotonic Regression (SIR) [14], and Ensemble Temperature Scaling (ETS) [33]. Scaling-binning combines the techniques of Platt Scaling and Histogram Binning. SIR employs linear interpolation based on isotonic regression, while ETS combines multiple temperature scalings for calibration, offering greater expressiveness than temperature scaling. Notably, all of these methods utilize raw predicted scores as input without taking field information into account.

2.3.2 Field-aware Methods. Field-aware methods integrate supplementary features to formulate calibration functions. NeuralCalib (FAC) [23] introduces an auxiliary module by utilizing neural networks and incorporates multiple field modeling. However, it does not address the challenge of shape miscalibration variance among different field values. AdaCalib (Ada) [28] learns an isotonic function based on posterior statistics and selects the most appropriate bin number for a single field value. However, AdaCalib does not encompass all fields. MBCT [12] employs trees to uncover more effective calibration across fields. However, due to its high computational complexity, calibration trees are unable to handle sparse fields, such as user ID and item ID, and do not adequately address discrepancies in shape calibration.

3 PROBLEM FORMULATION

In the context of online advertising systems, using CTR as an illustration (CVR follows the same principles), we have trained a neural predictor, denoted as $f_{uncalib}$, on a training dataset \mathcal{D}_{train} . This dataset includes all field values as inputs (x) and click responses (y), where $y = 0$ represents non-click events and $y = 1$ signifies click events. The neural predictor is capable of forecasting the likelihood of a click using the following formula.

$$\hat{p}_{uncalib} = f_{uncalib}(x) \quad (1)$$

To address the under- and over-estimation issues associated with the predicted scores generated by $f_{uncalib}$, we must train an additional calibrator, denoted as f_{calib} , while considering n distinct fields (Z_1, Z_2, \dots, Z_n) in a validation dataset. Our objective is for f_{calib} to predict the conditional expectation $E[y|x]$. Subsequently, the theoretical calibration error of f_{calib} with respect to the ground-truth under the l_p -norm is defined as:

$$TCE_p(f_{calib}) = (E_x[|E[y|x] - f_{calib}(x)|^p])^{\frac{1}{p}}. \quad (2)$$

The calibrator f_{calib} is considered to be perfectly calibrated when the theoretical calibration error $TCE_p(f_{calib})$ is zero. However, in fact perfect calibration is impossible in practice. Only approximate and asymptotic grouped calibrations are possible for finite and specific partitions of samples [10]. To test the performance of different calibrators, we will explain some related calibration metrics in EXPERIMENTS section.

4 METHODS

Under the requirement of multi-field calibration, both **shape** calibration and **value** calibration need to be performed simultaneously. Therefore, within the entire DESC architecture, we have designed separate modules, namely Shape Calibrator and Value Calibrator (Figure 3), to achieve **shape** calibration and **value** calibration. The final calibrated score is the product of these two parts:

$$\hat{p}_{calib} = \mathbb{S}(x) \cdot \mathbb{V}(x). \quad (3)$$

$\mathbb{S}(x)$ and $\mathbb{V}(x)$ refer to the shape calibrated score (the output of Shape Calibrator) and value calibrated score (the output of Value Calibrator), respectively. The input x consists of all n field values and non-calibrated scores $\hat{p}_{uncalib}$. The training loss function is the negative log-likelihood function.

$$\mathcal{L}(x, y) = -\frac{1}{|\mathcal{D}|} (y \cdot \log \hat{p}_{calib} + (1 - y) \cdot \log(1 - \hat{p}_{calib})) \quad (4)$$

In Section 4.1, we present the Shape Calibrator module, which is responsible for achieving shape calibration. In Section 4.2, we discuss the Value Calibrator module, which is designed to accomplish value calibration. In Section 4.3, we elaborate on the deployment of DESC in an online setting, outlining the necessary procedures and considerations.

4.1 Shape Calibrator

For multi-field calibration, the goal of Shape Calibrator is to ensure that: given input features x , we need to reduce the problems of over- and under-estimation across all intervals of pCTR (shape miscalibration).

In section 4.1.1, we pre-define a variety of basis functions to accommodate different shape requirements. Section 4.1.2 deals with the allocation of appropriate shape functions given specific field conditions. This section offers separate discussions on how shape allocation is managed for regular fields and sparse fields.

In section 4.1.3, when dealing with multiple fields, there may be conflicts in terms of the influence of different fields on calibration. Thus, we introduce a multi-field fusion mechanism named Multi-Field Shape Ensemble.

Collectively, sections 4.1.1 and 4.1.2 are referred to as the Single Field Shape Calibrator (SFSC), as depicted in Figure 3b.

4.1.1 Shape Pre-Define. In this section, we pre-define some basis calibration functions. Then, we merge the basis calibration functions into shape functions to enhance their expressive ability.

Basis calibration function $\mathcal{B}(x)$ satisfies the following conditions:

1. The function is monotonically non-decreasing and continuous in range $(0, 1)$.
2. When x approaches 0^+ , the limit of $\mathcal{B}(x)$ is 0, and when x approaches 1^- , the limit of $\mathcal{B}(x)$ is 1 (Equation 5).

$$\lim_{x \rightarrow 0^+} \mathcal{B}(x) = 0 \text{ and } \lim_{x \rightarrow 1^-} \mathcal{B}(x) = 1 \quad (5)$$

In Equation 6, we pre-define m basis functions consisting of p power functions, l logarithmic functions and s scaling functions. These functions exhibit different shape characteristics, and their shapes vary when the hyper-parameters (e.g. the coefficients in these basis calibration functions) are different. Compared to segmented linear functions in traditional calibration methods, including SIR, FAC, Ada, using basis calibration functions doesn't require data segmentation. In other words, shape learning can utilize all

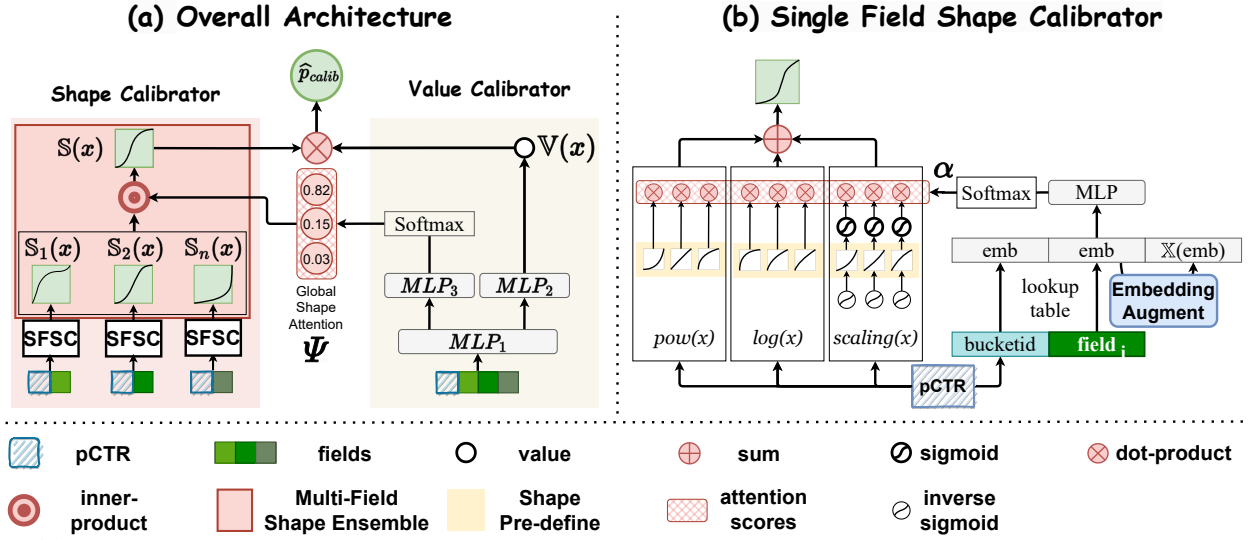


Figure 3: (a) Overall architecture of DESC, its input includes the non-calibrated pCTR and the original fields, and the final output is the calibrated pCTR. It is end-to-end trainable. (b) Single Field Shape Calibrator takes one field and the non-calibrated pCTR as inputs and outputs the calibrated shape score for this field.

samples for training, significantly enhancing the data utilization.

$$\mathcal{B}(x) = \underbrace{\{\mathcal{B}_1^{power}, \dots, \mathcal{B}_p^{power}\}}_{p \text{ power functions}} \underbrace{\{\mathcal{B}_1^{log}, \dots, \mathcal{B}_l^{log}\}}_{l \text{ log functions}} \underbrace{\{\mathcal{B}_1^{scaling}, \dots, \mathcal{B}_s^{scaling}\}}_{s \text{ scaling functions}} \quad (6)$$

$$\mathcal{B}_i^{power}(x; h_i) = x^{h_i} \quad (7)$$

$$\mathcal{B}_i^{log}(x; v_i) = \frac{\log(1 + v_i \cdot x)}{\log(1 + v_i)} \quad (8)$$

$$\mathcal{B}_i^{scaling}(x; a_i) = \sigma(\sigma^{-1}(x) \cdot a_i), \quad (9)$$

$$\text{where } \sigma(x) = \frac{1}{1 + \exp(-x)} \text{ and } \sigma^{-1}(x) = \log\left(\frac{x}{1-x}\right) \quad (10)$$

h_i, v_i and a_i ($h_i, v_i, a_i \in \mathbf{R}^+$) are parameters of basis calibration functions. We pre-define these parameters using equally spaced floats (e.g. [0.3, 0.5, 0.7, 0.9]) for each type of basis calibration function.

However, $\mathcal{B}(x)$ can only represent simple shapes, and complex shapes can be composed of simple shapes, as shown in Figure 4. Therefore, we need to combine these basis calibration functions through weighted summation to create shape function $\mathbb{S}_i(x)$ capable of representing complex shapes for i -th field, as shown in Equation 11, where α_i^j refers to the attention weight of j -th basis function for i -th field, which will be explained in next section.

$$\mathbb{S}_i(x) = \sum_{j=1}^m \alpha_i^j \cdot \mathcal{B}_j(x), \quad \mathcal{B}_j(x) \in \mathcal{B}(x) \quad (11)$$

4.1.2 Shape Allocation. In shape allocation, we allocate suitable shape functions based on feature values. These features include two parts: pCTR bucket feature and original field features. Introducing pCTR bucket feature allows for better shape allocation within different pCTR intervals. The specific steps are as follows:

Step1. We pre-define the embedding size for each feature. Each one-hot feature (including pCTR bucket feature $bucket_{\hat{p}_{uncalib}}$ and original field Z_i) is projected into a fixed-size dense embedding, such as $\mathbf{b}_{\hat{p}_{uncalib}}$ and \mathbf{e}_i . The bucket size of $bucket_{\hat{p}_{uncalib}}$ is assigned as 100.

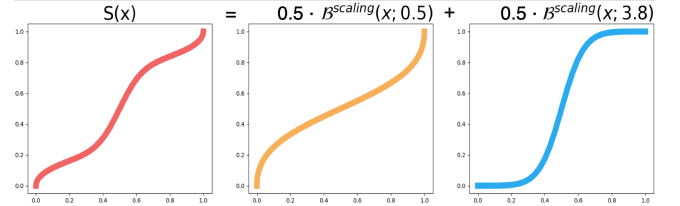


Figure 4: Complex shape can be composed of simple shapes.

Step2. We concatenate embedding vectors into a Multi-Layer Perceptron (MLP), followed by a softmax operation, the output α_i size of softmax is $1 \times m$, with α_i^1 to α_i^m , same as the number of pre-defined basis functions.

$$\alpha_i = \text{Softmax}(\text{MLP}(\mathbf{b}_{\hat{p}_{uncalib}}, \mathbf{e}_i)) \quad (12)$$

Step3. Finally, we obtain the output value of the Shape Calibrator $\mathbb{S}_i(x)$ for Z_i shown in the previous Equation 11.

In the shape allocation stage, the expressive ability of embedding directly affects the ability of allocating shapes. For sparse fields, we enhance the expressive ability of embeddings by using self-attention. The specific formula is shown in following formula, where d is the dimension of \mathbf{e} and n is the number of fields.

$$\mathbb{X}(\mathbf{e}_i) = \sum_{j=1}^n (\text{Softmax}\left(\frac{\mathbf{e}_i \cdot \mathbf{e}_j^T}{\sqrt{d}}\right) \cdot \mathbf{e}_j) \mathbf{1}_{[i \neq j]} \quad (13)$$

That means: for more similar fields, their miscalibration distributions will be similar. If the semantics between two embeddings \mathbf{e}_i and \mathbf{e}_j is similar, then the corresponding weight is also relatively large.

$$\alpha_i = \text{Softmax}(\text{MLP}(\mathbf{b}_{\hat{p}_{uncalib}}, \mathbf{e}_i, \mathbb{X}(\mathbf{e}_i))) \quad (14)$$

Next, we concatenate the original embedding \mathbf{e}_i , the enhanced output embedding $\mathbb{X}(\mathbf{e}_i)$, and the pCTR bucket embedding $\mathbf{b}_{\hat{p}_{uncalib}}$. Then, following the same process as in the shape allocation stage, we generate the attention for shape allocation α_i and perform the final fusion.

4.1.3 Multi-Field Shape Ensemble. Different calibration values for different fields can conflict with each other. For example, there is a scenario where 19 to 26-year-old users demand for women’s shoes. Under the item category field of "women’s shoes", the non-calibrated model behaves 30% over-estimation of pCTR in the 0.01 to 0.03 range. However, under the user age field of "19 to 26", there’s a 20% under-estimation of pCTR in the same 0.01 to 0.03 range.

Consequently, we not only need to perform shape calibration on individual field but also need to globally harmonize the outputs of shape calibrators for different fields. This helps reduce calibration errors at a global level.

We use Global Shape Attention to combine the output results obtained from different fields (Figure 3a). Global Shape Attention, denoted as Ψ , is derived from the Global Shape Attention Generator module (details will be elaborated in section 4.2.2). The size of Ψ is $1 \times n$, with $\Psi_i \in [0, 1]$, and $\sum_{i=1}^n \Psi_i = 1$. The fusion formula is as follows, where there are a total of n fields, and $\mathbb{S}_i(x)$ represents the output of the shape calibrator for i -th field.

$$\mathbb{S}(x) = \sum_{i=1}^n \mathbb{S}_i(x) \cdot \Psi_i \quad (15)$$

We finally obtain the output of Global Shape Calibrator: $\mathbb{S}(x)$.

4.2 Value Calibrator

The goal of the Value Calibrator is to ensure that, for each sample x , there is no overall over- or under-estimation (value calibration). We use all fields for Value Calibrator to achieve the best overall performance, as described in section 4.2.1. Considering all fields allows for the excellent allocation of shapes for each field, we use global shape attention depicted in section 4.2.2.

4.2.1 Global Field Value Calibrator. Global Field Value Calibrator encompasses all the necessary information of the fields concerned. These input fields are projected into fixed-size dense representations, which are fed into a neural network (the form of the neural network is not restricted, here we use MLP). Then we get the middle output *hiddenLayer* and the final output $\mathbb{V}(x)$ for the Global Field Value Calibrator. Finally, by combining $\mathbb{V}(x)$ and $\mathbb{S}(x)$, we obtain the final calibrated output $\hat{p}_{calib} = \mathbb{S}(x) \cdot \mathbb{V}(x)$.

$$hiddenLayer = MLP_1(Concat(\mathbf{b}_{p_{uncalib}}, \mathbf{e}_1, \mathbf{e}_2, \dots, \mathbf{e}_n)) \quad (16)$$

$$\mathbb{V}(x) = MLP_2(hiddenLayer) \quad (17)$$

4.2.2 Global Shape Attention Generator. The Global Field Value Calibrator not only produces the final output but also yields valuable intermediate representation. In this context, we use the intermediate representation *hiddenLayer* as input of Equation 18, which can effectively learn information from all fields. After passing through a MLP and softmax layer, it produces Global Shape Attention Score Ψ with a size equal to the number of fields n . In the Shape Calibration stage, the output produced by each field Z_i is multiplied by its corresponding score Ψ_i and summed to obtain the final Shape Calibration Score.

$$\Psi = Softmax(MLP_3(hiddenLayer)) \quad (18)$$

4.3 Online Deployment

The overall framework of the online service using the DESC calibration method in our industrial advertising system is shown in Figure 5. When a real-time user request comes, all candidate items are recalled and predicted with pCTRs by a non-calibration model

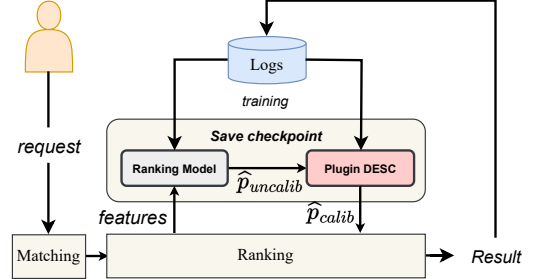


Figure 5: Real-Time calibration system used DESC method for CXR (CTR/CVR) task in our industrial advertising system.

(ranking model). Then DESC model calibrates the pCTRs considering different field values, including user, item, and context features. In detail, the input x of DESC has two parts: different field values and its non-calibrated score $\hat{p}_{uncalib}$. DESC uses a light neural network to output the calibrated score \hat{p}_{calib} , which is then used to sort the final ranks for all candidate items. We have integrated the DESC method as a plugin into the ranking model to reduce maintenance costs while only adding a little more time for online inference.

5 EXPERIMENTS

5.1 Experimental Setup

5.1.1 Datasets. To validate the effectiveness of our proposed DESC method, we conduct experiments on two public datasets (**AliCCP** and **CRITEO** for CTR prediction tasks) and one industrial dataset (**Shopee** for CVR prediction task). **CRITEO** display advertising data², which consists of 46 million samples. We split the samples into 28 million samples as training set (\mathcal{D}_{train}), 9 million samples as validation set (\mathcal{D}_{dev}) and other 9 million samples as testing set (\mathcal{D}_{test}). **AliCCP** (Alibaba Click and Conversion Prediction) [20]³ contains 80 million samples. We split these samples with the proportion 2:1:1 to \mathcal{D}_{train} , \mathcal{D}_{dev} and \mathcal{D}_{test} . To test DESC method on CVR prediction task, we collect the conversion logs from the **Shopee**’s online advertising system. It contains 100 million samples, where the first 60 million for \mathcal{D}_{train} , the next 20 million for \mathcal{D}_{dev} and the last 20 million for \mathcal{D}_{test} .

5.1.2 Competing Methods. Several representative calibration methods are used as competitors. We tested several competitive methods, including parametric methods, non-parametric methods, non-field-aware hybrid methods and field-aware hybrid methods. Parametric method contains Platt Scaling (PS) [24]. Non-parametric method contains Histogram Binning (HB) [30] and Isotonic Regression (IR) [31]. Non-field-aware method contains Smooth Isotonic Regression (SIR) [14] and Ensemble Temperature Scaling (ETS) [33]. Field-aware method contains FAC [23], Ada [28] and MBCT [12].

We use DeepFM [9] to train the non-calibrated models with all fields in \mathcal{D}_{train} , and predict the non-calibrated scores in \mathcal{D}_{dev} and \mathcal{D}_{test} .

All calibration methods are trained using samples of \mathcal{D}_{dev} and are tested using samples of \mathcal{D}_{test} .

5.1.3 Parameter Configuration. For all neural calibrators, including FAC, Ada and DESC, we use Adam as the optimizer with a learning

²<https://www.kaggle.com/c/criteo-display-ad-challenge>

³<https://tianchi.aliyun.com/datalab/dataSet.html?dataId=408>

rate of $1e-3$ and batch size of 16,384. For the embedding size of field value d , both FAC and Ada are set as 256 while for DESC, it is 128 because it obtains a better result. For FAC, we set the number of bins to 100 while for Ada, the candidate set of bin numbers is set $\{2, 4, 8\}$ following in [28]. For DESC, the number of basis functions m is 48 (the numbers of the three types of basis functions are both 16), and the numbers of fields n are 26, 23 and 10 for Criteo, AliCCP and Industrial dataset, respectively. For MBCT, we set the same hyperparameters according to the paper.

5.1.4 Compared Metrics. Two commonly used metrics, F-RCE (Field RCE) and F-ECE (Field ECE) for each field Z_i are used. To calculate the F-RCE of i -th field (shown in Equation 19), we use the testing dataset \mathcal{D}_{test} (for simplicity, \mathcal{D} refers to \mathcal{D}_{test} here) consisting of (x^j, y^j) , where x^j and y^j mean the input features with different fields and clicked label of j -th sample. The subset of \mathcal{D}^z has the samples with the same value z for i -th field. F-RCE of i -th field evaluates the deviation level of each sample's calibrated probability \hat{p}_{calib}^j considering j -th field.

Another metric is the F-ECE of i -th field. As shown in Equation 20, it can be calculated for each subset \mathcal{D}^z of samples with the same value in i -th field. We can calculate the subset of F-ECE (shown in Equation 21) by partitioning predictions into M equally-spaced bins and taking a weighted average of the difference between bins' accuracy and confidence. In detail, firstly we sort the samples by the non-calibrated scores $\hat{p}_{uncalib}^j$. Then all samples are grouped into M interval bins. For all samples (B_m) in m -th bin, we calculate the accuracy and confidence, where the accuracy is the average of labels and the confidence is the average of calibrated scores.

$$F-RCE_i = \frac{1}{|\mathcal{D}|} \sum_{z \in Z_i} \frac{|\sum_{(x^j, y^j) \in \mathcal{D}^z} (y^j - \hat{p}_{calib}^j)|}{\frac{1}{|\mathcal{D}^z|} \sum_{(x^j, y^j) \in \mathcal{D}^z} y^j} \quad (19)$$

$$F-ECE_i @ M = \frac{1}{|\mathcal{D}|} \sum_{z \in Z_i} |\mathcal{D}^z| \cdot (F-ECE_{\mathcal{D}^z} @ M) \quad (20)$$

$$F-ECE_{\mathcal{D}^z} @ M = \sum_{m=1}^M \frac{|B_m|}{|\mathcal{D}^z|} |acc(B_m) - conf(B_m)| \quad (21)$$

$$acc(B_m) = \frac{1}{|B_m|} \sum_{j \in B_m} y^j, \quad conf(B_m) = \frac{1}{|B_m|} \sum_{j \in B_m} \hat{p}_{calib}^j \quad (22)$$

As explained that the traditional field-aware calibration methods, such as FAC [23] and Ada [28], only consider one field to calibrate, these methods do not take into account the influence of other fields on the calibration results. We found that the calibration results from these models only training on one field perform poorly on other fields. So we use the Multi-Field RCE (MF-RCE) and Multi-Field ECE (MF-ECE) on all fields to compare different methods as follows:

$$MF-RCE = \frac{1}{n} \sum_i F-RCE_i \quad (23)$$

$$MF-ECE @ M = \frac{1}{n} \sum_i F-ECE_i @ M, \quad (24)$$

where n is the number of fields.

We use F-RCE and F-ECE as the primary empirical metrics to compare the calibration errors of different calibration methods on one field and MF-RCE and MF-ECE to test on all fields. Besides, we also report the overall ranking performance by using AUC and Log-loss metrics. Since PCOC (Predicted Click Over Click) [7, 11] and ECE (Expected Calibration Error) [12] indicators can be

achieved well for all competing methods, and F-ECE and MF-ECE, as compared to the traditional ECE, can provide a finer-grained representation of calibration error in the context of field-aware problems, PCOC and ECE are not listed in the main results.

5.2 Main Results

5.2.1 Results on One Field. As other hybrid field-aware based methods only consider one field to calibrate, we compare our proposed method in one field in the same way. We select the field of "C2" (577 unique values) in Criteo, "853" (39,979 unique values) in AliCCP and "item ID" (5 million unique values) in Industrial data to perform our experiments. As shown in Table 1, the AUCs of all calibrators are higher than the uncalibrator while all other calibration-related metrics (F-ECE, F-RCE) of calibrators are smaller than the uncalibrator, which shows that the calibration methods can improve the accuracy of pCTR while maintaining a certain increase in ranking performance. Specially, by fusing multiple fields in shape allocation and shape augmentation, our proposed DESC can achieve much smaller calibration errors compared to other competitors even in one field evaluation. It's worth explaining that DESC performs much better than other competitors in industrial data than public data. The reason is that DESC behaves better in calibration performance in this scene where the data sparsity is more serious in practical industrial data.

5.2.2 Results on All Fields. As DESC can consider the effects of different fields on calibration, we need to evaluate its performance on all fields. As shown in Table 2, the conclusion is consistent with the smallest calibration errors on all three datasets.

5.3 In-Depth Analysis

5.3.1 Model Structure Ablation Experiment for DESC. We perform some model structure ablation experiments to validate the significance and effectiveness.

(1) Ablation Experiment of Shape Calibrator. To evaluate the effectiveness of the Shape Calibrator and Value Calibrator, we delete the corresponding module and left the other parts unchanged. Firstly, we delete the Shape Calibrator sub-module, the AUC reduces to 0.6602 while the metrics of MF-RCE and MF-ECE@3 on all fields are slightly larger than DESC with 0.1434 and 0.0120 (first line on Table. 3).

(2) Ablation Experiment of Value Calibrator. Secondly, we delete another sub-module, the Value Calibrator. The phenomenon is almost the same, with 0.6761 of AUC, and 0.1398 and 0.0119 of MF-RCE and MF-ECE@3 on all fields (second line on Table. 3).

(3) Ablation Experiment of Multi-Field Shape Ensemble. In METHODS section, we have emphasized that shape calibration needs to consider multiple fields because different fields and values can have numerous different shapes. Then, we only use mean-pooling to compute the final predicted result considering different fields (Ψ_i is all the same with $1/n$ in Equation 15). The results are still inferior as shown in the third line in Table. 3.

(4) Ablation Experiment of pCTR Bucket Feature. The pCTR bucket feature is concatenated with the field embedding to calculate the shape allocation weights in DESC (Equation 14). Then we delete the pCTR bucket feature (fourth line on Table. 3) to verify that different pCTR values can also have effects on the calibration shape.

Table 1: Results of different methods for calibrating CTR predictive models on public and industrial datasets for one field.

Type	Method	Criteo				AliCCP				Industrial Data			
		AUC ↑	Log-loss ↓	F-RCE ↓	F-ECE@3 ↓	AUC ↑	Log-loss ↓	F-RCE ↓	F-ECE@3 ↓	AUC ↑	Log-loss ↓	F-RCE ↓	F-ECE@3 ↓
No Calib.	N/A	0.7949	0.4559	0.0426	0.0119	0.6130	0.1611	0.0876	0.0135	0.8613	0.5212	0.0743	0.0253
Non-Param	HB	0.7944	0.4562	0.0328	0.0112	0.6128	0.1621	0.0852	0.0130	0.8610	0.5218	0.0669	0.0204
	IR	0.7949	0.4559	0.0320	0.0110	0.6130	0.1611	0.0843	0.0132	0.8613	0.5212	0.0665	0.0202
Param	PS	0.7949	0.4559	0.0301	0.0105	0.6130	0.1611	0.0841	0.0128	0.8613	0.5212	0.0660	0.0201
Non-Field-Aware	SIR	0.7949	0.4559	0.0300	0.0097	0.6130	0.1611	0.0836	0.0127	0.8613	0.5211	0.0660	0.0201
	ETS	0.7949	0.4559	0.0293	0.0095	0.6130	0.1611	0.0837	0.0127	0.8613	0.5212	0.0661	0.0199
Field-Aware	FAC	0.7991	0.4523	0.0265	0.0087	0.6751	0.1571	0.0829	0.0123	0.8634	0.5203	0.0402	0.0163
	Ada	0.7992	0.4521	0.0273	0.0089	0.6752	0.1568	0.0832	0.0125	0.8639	0.5201	0.0413	0.0170
	MBCT	0.7951	0.4550	0.0248	0.0095	0.6742	0.1611	0.0828	0.0128	0.8621	0.5209	0.0409	0.0175
	DESC	0.7992	0.4522	0.0203	0.0080	0.6774	0.1566	0.0821	0.0120	0.8641	0.5192	0.0307	0.0132

Table 2: Results of different methods for calibrating CTR predictive models on public and industrial datasets for all fields.

Type	Method	Criteo		AliCCP		Industrial Data	
		MF-RCE ↓	MF-ECE@3 ↓	MF-RCE ↓	MF-ECE@3 ↓	MF-RCE ↓	MF-ECE@3 ↓
No Calib.	N/A	0.0702	0.0142	0.1492	0.0143	0.0793	0.0370
Non-Param	HB	0.0692	0.0134	0.1430	0.0135	0.0779	0.0250
	IR	0.0688	0.0131	0.1427	0.0131	0.0766	0.0249
Param	PS	0.0685	0.0130	0.1420	0.0129	0.0765	0.0248
Non-Field-Aware	SIR	0.0686	0.0131	0.1422	0.0130	0.0764	0.0247
	ETS	0.0683	0.0127	0.1470	0.0129	0.0761	0.0248
Field-Aware	FAC	0.0517	0.0101	0.1321	0.0120	0.0412	0.0183
	Ada	0.0501	0.0102	0.1338	0.0122	0.0415	0.0180
	MBCT	0.0660	0.0104	0.1357	0.0125	0.0430	0.0192
	DESC	0.0489	0.0099	0.1264	0.0115	0.03606	0.0132

Table 3: Ablation study of DESC on AliCCP.

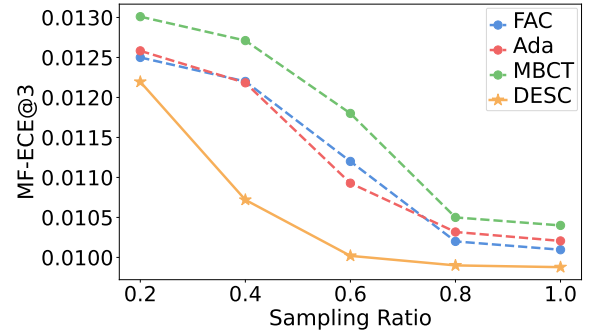
Type	AUC ↑	Log-loss ↓	MF-RCE ↓	MF-ECE@3 ↓
w/o Shape Calibrator	0.6602	0.1581	0.1434	0.0120
w/o Value Calibrator	0.6761	0.1567	0.1398	0.0119
w/o Multi-Field Shape Ensemble	0.6755	0.1568	0.1324	0.0116
w/o pCTR Bucket Feature	0.6764	0.1567	0.1391	0.0120
w/o Embedding Augment	0.6764	0.1567	0.1398	0.0119
DESC	0.6774	0.1566	0.1264	0.0115

(5) **Ablation Experiment of Embedding Augmentation.** To enhance the expressive ability of embeddings, the self-attention mechanism is used. Then we delete this part by using the original Equation 12 rather than Equation 14. The fifth line on Table. 3 shows that the embedding augmentation mechanism can enhance the representational power of embedding.

5.3.2 *DESC exhibits a stronger data utilization capability.* In this part, we analyze the data utilization capabilities of different calibrators from both a global perspective (overall down sampling) and an individual perspective (field value sample quantity).

(1) **Overall Down Sampling** We further conducted experiments to compare the calibration performance of four different hybrid field-aware methods (FAC, Ada, MBCT and DESC) across various sampling ratios. As shown in Figure 6, DESC exhibits a distinct lower MF-ECE in the context of varying sampling ratios. In a global perspective, this demonstrates that DESC exhibits a stronger data utilization capability.

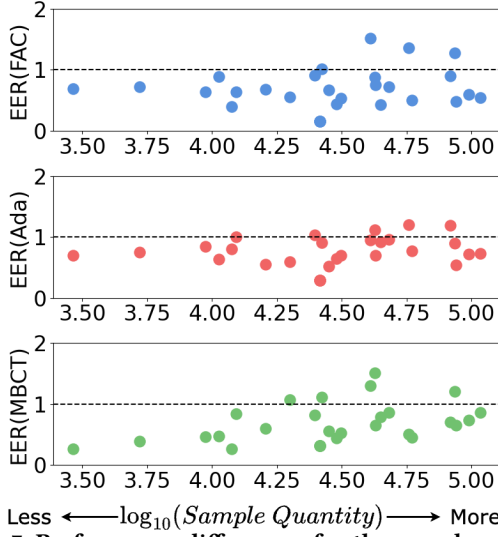
(2) **Field Value Sample Quantity.** We analysis the performance differences among MBCT, FAC, Ada and DESC at sample quantity aspect. We set the quantity of samples with a specific field value

**Figure 6: Down sampling analysis in CRITEO.**

(for the convenience of display, we use $\log_{10}(x)$ as the x-axis and EER_{Calib} (Except Calibration Error Ratio) as the y-axis (the smaller EER_{Calib} is, the better DESC is compared with other calibrators), as shown in Figure 7.

$$EER_{Calib} = \frac{ECE_{DESC}}{ECE_{Calib}}, Calib \in \{MBCT, FAC, Ada\} \quad (25)$$

ECE (Expected Calibration Error) [12] is used as the calibration error to explain the results. The ECE value ranges from $(0, +\infty]$. The higher ECE value indicates higher calibration error and worse performance. We can find that for the samples with small sized of number, EER is less than 1, which means, from an individual perspective, that DESC possesses a stronger data utilization capability.



Less $\leftarrow \log_{10}(\text{Sample Quantity}) \rightarrow$ More
Figure 7: Performance differences for the sample quantity of the field value.

5.3.3 *DESC Can Adapt to Complex Miscalibration Shapes.* We analyze the performance differences among MBCT, FAC, Ada and DESC at shape complexity.

From the perspective of pCTR, we divide the estimated pCTR values into bins either with equal frequency or equal interval, and each bin can calculate the PCOC (Predicted Click Over Click) [7, 11] to describe the over- and under-estimation within that bin.

For some cases, the over- and under-estimation within each bin are close, while in other cases, there is a significant difference in over- and under-estimation for each bin. We define the "Miscalibration Complexity" metric to characterize the disparity in over- and under-estimation across different pCTR bins. We selected all field values for a subset of fields. For field Z with a value v , the samples are divided into Q ($Q > 1$) bins. The miscalibration complexity is denoted as $\mathbb{D}_{Z,v}$ as follows:

$$\mathbb{D}_{Z,v} = \frac{1}{Q-1} \sum_{bin=1}^{Q-1} |PCOC_{bin+1} - PCOC_{bin}|. \quad (26)$$

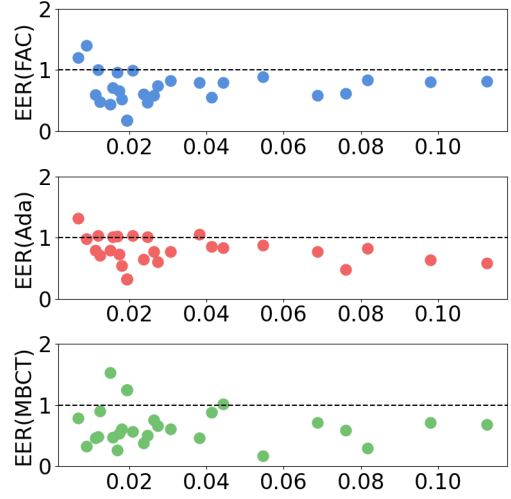
In general, the higher the miscalibration complexity, the higher the disparity in over- and under-estimation within the bins. For a calibrator, a higher miscalibration complexity indicates a greater calibration challenge. On one hand, it requires higher precision in shaping the accuracy of the calibration, and on the other hand, an excessive reliance on posterior data can compromise the generalization capability of the calibrator.

We still use the ECE metric to characterize the calibration error of different calibrators under the specific field value. We compare MBCT, FAC, Ada, and DESC and obtain the EER_{Calib} .

For each calibrator and each field value, there is a corresponding $\mathbb{D}_{Z,v}$ value as the x-axis and EER_{Calib} as the y-axis. As shown in Figure 8, we can observe that in the high $\mathbb{D}_{Z,v}$ range, all EER_{Calib} values are less than 1, which indicates that DESC always performs better in conditions of complex shapes compared to other methods.

5.4 Online Results

To prove the effectiveness of the proposed method, we further conduct real-world online experiments. We feed item ID with 5 million



Easy \leftarrow Miscalibration Complexity \rightarrow Complex
Figure 8: Performance differences for miscalibration complexity aspect.

unique values, category ID with 5,000 unique values, bidding type, time, raw predict score and other features into DESC. Then the model is deployed for online pCVR calibration on Shopee's advertising system. For the online A/B test, we build two experimental buckets, each with ten percent of the traffic. One bucket was configured with SIR [14] as the control group, while the other was configured with DESC as the experimental group. We use the two significant important business metrics CVR (Conversion Rate) and GMV (Gross Merchandise Volume) to evaluate our calibration effectiveness. The online results over a 7-day period indicated that DESC brings +2.5% on CVR and +4.0% on GMV compared to SIR. These improvements verify the effectiveness and business values of DESC in practical advertising system.

6 DISCUSSION

We propose a new calibration approach named DESC. Firstly, we put forward multiple types of functions (e.g., power function, scaling function, logarithmic function) as the basis functions. Secondly, we allocate the appropriate basis functions to combine the shape function given the specific field and specific value. Finally, all fields are concatenated and used to calculate the weight for the calibration value from each field, which can further improve the accuracy of pCTR on multiple fields. Both offline and online experiments verify that DESC achieves significant improvement. In future work, we should explore the performance of our proposed method on other machine learning tasks except CXR task. Also, we need to study the reasons of miscalibration error in these machine learning tasks, especially for CXR task, and find new technology (e.g. data augment, multi-tasking learning) to further improve the performance.

REFERENCES

- [1] Antonio Bella, Cèsar Ferri, José Hernández-Orallo, and María José Ramírez-Quintana. 2010. Calibration of machine learning models. In *Handbook of Research on Machine Learning Applications and Trends: Algorithms, Methods, and Techniques*. IGI Global, 128–146.

- [2] Weijie Bian, Kailun Wu, Lejian Ren, Qi Pi, Yujing Zhang, Can Xiao, Xiang-Rong Sheng, Yong-Nan Zhu, Zhangming Chan, Na Mou, et al. 2022. CAN: feature co-action network for click-through rate prediction. In *Proceedings of the fifteenth ACM international conference on web search and data mining*. 57–65.
- [3] Heng-Tze Cheng, Levent Koc, Jeremiah Harmsen, Tal Shaked, Tushar Chandra, Hrishu Aradhye, Glen Anderson, Greg Corrado, Wei Chai, Mustafa Ispir, et al. 2016. Wide & deep learning for recommender systems. In *Proceedings of the 1st workshop on deep learning for recommender systems*. 7–10.
- [4] James Davidson, Benjamin Liebald, Junning Liu, Palash Nandy, Taylor Van Vleet, Ullas Gargi, Sujoy Gupta, Yu He, Mike Lambert, Blake Livingston, et al. 2010. The YouTube video recommendation system. In *Proceedings of the fourth ACM conference on Recommender systems*. 293–296.
- [5] Chao Deng, Hao Wang, Qing Tan, Jian Xu, and Kun Gai. 2021. Calibrating user response predictions in online advertising. In *Machine Learning and Knowledge Discovery in Databases: Applied Data Science Track: European Conference, ECML PKDD 2020, Ghent, Belgium, September 14–18, 2020, Proceedings, Part IV*. Springer, 208–223.
- [6] Chao Du, Zhifeng Gao, Shuo Yuan, Lining Gao, Ziyang Li, Yifan Zeng, Xiaoqiang Zhu, Jian Xu, Kun Gai, and Kuang-Chih Lee. 2021. Exploration in online advertising systems with deep uncertainty-aware learning. In *Proceedings of the 27th ACM SIGKDD Conference on Knowledge Discovery & Data Mining*. 2792–2801.
- [7] Thore Graepel, Joaquin Quinonero Candela, Thomas Borchert, and Ralf Herbrich. 2010. Web-scale bayesian click-through rate prediction for sponsored search advertising in microsoft's bing search engine. Omnipress.
- [8] Chuan Guo, Geoff Pleiss, Yu Sun, and Kilian Q Weinberger. 2017. On calibration of modern neural networks. In *International conference on machine learning*. PMLR, 1321–1330.
- [9] Huifeng Guo, Ruiming Tang, Yunming Ye, Zhenguo Li, and Xiuqiang He. 2017. DeepFM: a factorization-machine based neural network for CTR prediction. *arXiv preprint arXiv:1703.04247* (2017).
- [10] Chirag Gupta, Aleksandr Podkopaev, and Aaditya Ramdas. 2020. Distribution-free binary classification: prediction sets, confidence intervals and calibration. *Advances in Neural Information Processing Systems* 33 (2020), 3711–3723.
- [11] Xinran He, Junfeng Pan, Ou Jin, Tianbing Xu, Bo Liu, Tao Xu, Yanxin Shi, Antoine Atallah, Ralf Herbrich, Stuart Bowers, et al. 2014. Practical lessons from predicting clicks on ads at facebook. In *Proceedings of the eighth international workshop on data mining for online advertising*. 1–9.
- [12] Siguang Huang, Yunli Wang, Lili Mou, Huayue Zhang, Han Zhu, Chuan Yu, and Bo Zheng. 2022. MBCT: Tree-Based Feature-Aware Binning for Individual Uncertainty Calibration. In *Proceedings of the ACM Web Conference 2022*. 2236–2246.
- [13] Tongwen Huang, Zhiqi Zhang, and Junlin Zhang. 2019. FiBiNET: combining feature importance and bilinear feature interaction for click-through rate prediction. In *Proceedings of the 13th ACM Conference on Recommender Systems*. 169–177.
- [14] Xiaoqian Jiang, Melanie Osl, Jihoon Kim, and Lucila Ohno-Machado. 2011. Smooth isotonic regression: a new method to calibrate predictive models. *AMIA Summits on Translational Science Proceedings* 2011 (2011), 16.
- [15] Kevin B Korb. 1999. Calibration and the evaluation of predictive learners. In *Proceedings of the Sixteenth International Joint Conference on Artificial Intelligence*. Citeseer, 73–77.
- [16] Meelis Kull, Miquel Perello Nieto, Markus Kängsepp, Telmo Silva Filho, Hao Song, and Peter Flach. 2019. Beyond temperature scaling: Obtaining well-calibrated multi-class probabilities with dirichlet calibration. *Advances in neural information processing systems* 32 (2019).
- [17] Meelis Kull, Telmo Silva Filho, and Peter Flach. 2017. Beta calibration: a well-founded and easily implemented improvement on logistic calibration for binary classifiers. In *Artificial Intelligence and Statistics*. PMLR, 623–631.
- [18] Ananya Kumar, Percy S Liang, and Tengyu Ma. 2019. Verified uncertainty calibration. *Advances in Neural Information Processing Systems* 32 (2019).
- [19] Wonbin Kweon, SeongKu Kang, and Hwanjo Yu. 2022. Obtaining Calibrated Probabilities with Personalized Ranking Models. In *Proceedings of the AAAI Conference on Artificial Intelligence*, Vol. 36. 4083–4091.
- [20] Xiao Ma, Liqin Zhao, Guan Huang, Zhi Wang, Zelin Hu, Xiaoqiang Zhu, and Kun Gai. 2018. Entire space multi-task model: An effective approach for estimating post-click conversion rate. In *The 41st International ACM SIGIR Conference on Research & Development in Information Retrieval*. 1137–1140.
- [21] Dang Minh Nguyen, Chenfei Wang, Yan Shen, and Yifan Zeng. 2023. LightSAGE: Graph Neural Networks for Large Scale Item Retrieval in Shopee's Advertisement Recommendation. In *Proceedings of the 17th ACM Conference on Recommender Systems*. 334–337.
- [22] Yaniv Ovadia, Emily Fertig, Jie Ren, Zachary Nado, David Sculley, Sebastian Nowozin, Joshua Dillon, Balaji Lakshminarayanan, and Jasper Snoek. 2019. Can you trust your model's uncertainty? evaluating predictive uncertainty under dataset shift. *Advances in neural information processing systems* 32 (2019).
- [23] Feiyang Pan, Xiang Ao, Pingzhong Tang, Min Lu, Dapeng Liu, Lei Xiao, and Qing He. 2020. Field-aware calibration: a simple and empirically strong method for reliable probabilistic predictions. In *Proceedings of The Web Conference 2020*. 729–739.
- [24] John Platt et al. 1999. Probabilistic outputs for support vector machines and comparissons to regularized likelihood methods. *Advances in large margin classifiers* 10, 3 (1999), 61–74.
- [25] Ying Shan, T Ryan Hoens, Jian Jiao, Haijing Wang, Dong Yu, and JC Mao. 2016. Deep crossing: Web-scale modeling without manually crafted combinatorial features. In *Proceedings of the 22nd ACM SIGKDD international conference on knowledge discovery and data mining*. 255–262.
- [26] Jizhe Wang, Pipei Huang, Huan Zhao, Zhibo Zhang, Binqiang Zhao, and Dik Lun Lee. 2018. Billion-scale commodity embedding for e-commerce recommendation in alibaba. In *Proceedings of the 24th ACM SIGKDD international conference on knowledge discovery & data mining*. 839–848.
- [27] Zhiqiang Wang, Qingyun She, and Junlin Zhang. 2021. MaskNet: Introducing feature-wise multiplication to CTR ranking models by instance-guided mask. *arXiv preprint arXiv:2102.07619* (2021).
- [28] Penghui Wei, Weimin Zhang, Ruijie Hou, Jinquan Liu, Shaoguo Liu, Liang Wang, and Bo Zheng. 2022. Posterior Probability Matters: Doubly-Adaptive Calibration for Neural Predictions in Online Advertising. In *Proceedings of the 45th International ACM SIGIR Conference on Research and Development in Information Retrieval*. 2645–2649.
- [29] Hao Yang, Ziliang Wang, Weijie Bian, and Yifan Zeng. 2023. Practice on Effectively Extracting NLP Features for Click-Through Rate Prediction. In *Proceedings of the 32nd ACM International Conference on Information and Knowledge Management*. 4887–4893.
- [30] Bianca Zadrozny and Charles Elkan. 2001. Obtaining calibrated probability estimates from decision trees and naive bayesian classifiers. In *Icml*, Vol. 1. 609–616.
- [31] Bianca Zadrozny and Charles Elkan. 2002. Transforming classifier scores into accurate multiclass probability estimates. In *Proceedings of the eighth ACM SIGKDD international conference on Knowledge discovery and data mining*. 694–699.
- [32] Shuangfei Zhai, Keng-hao Chang, Ruofei Zhang, and Zhongfei Mark Zhang. 2016. Deepintent: Learning attentions for online advertising with recurrent neural networks. In *Proceedings of the 22nd ACM SIGKDD international conference on knowledge discovery and data mining*. 1295–1304.
- [33] Jize Zhang, Bhavya Kaikhura, and T Yong-Jin Han. 2020. Mix-n-match: Ensemble and compositional methods for uncertainty calibration in deep learning. In *International conference on machine learning*. PMLR, 11117–11128.
- [34] Han Zhu, Junqi Jin, Chang Tan, Fei Pan, Yifan Zeng, Han Li, and Kun Gai. 2017. Optimized cost per click in taobao display advertising. In *Proceedings of the 23rd ACM SIGKDD international conference on knowledge discovery and data mining*. 2191–2200.